AIMS Biophysics, 3(3): 398-414.
DOI: 10.3934/biophy.2016.3.398
Received: 18 July 2016
Accepted: 21 August 2016
Published: 29 August 2016

http://www.aimspress.com/journal/biophysics

Research article

Continuous-flow sorting of microalgae cells based on lipid content by high frequency dielectrophoresis

Hanieh Hadady [1], Doug Redelman [2], Sage R. Hiibel [3], and Emil J. Geiger[1,*]

[1] Mechanical Engineering Department, University of Nevada, Reno, USA
[2] Physiology and Cell Biology Molecular Bioscience, University of Nevada, School of Medicine, Reno, USA
[3] Civil and Environmental Engineering Department, University of Nevada, Reno, USA

* **Correspondence:** E-mail: ejg@unr.edu; Tel: +775-784-6931; Fax: +775-784-1701.

Abstract: This paper presents a continuous-flow cell screening device to isolate and separate microalgae cells (*Chlamydomonas reinhardtii*) based on lipid content using high frequency (50 MHz) dielectrophoresis. This device enables screening of microalgae due to the balance between lateral DEP forces relative to hydrodynamic forces. Positive DEP force along with amplitude-modulated electric field exerted on the cells flowing over the planar interdigitated electrodes, manipulated low-lipid cell trajectories in a zigzag pattern. Theoretical modelling confirmed cell trajectories during sorting. Separation quantification and sensitivity analysis were conducted with time-course experiments and collected samples were analysed by flow cytometry. Experimental testing with nitrogen starved *dw15-1* (high-lipid, HL) and *pgd1* mutant (low-lipid, LL) strains were carried out at different time periods, and clear separation of the two populations was achieved. Experimental results demonstrated that three populations were produced during nitrogen starvation: HL, LL and low-chlorophyll (LC) populations. Presence of the LC population can affect the binary separation performance. The continuous-flow micro-separator can separate 74% of the HL and 75% of the LL out of the starting sample using a 50 MHz, 30 voltages peak-to-peak AC electric field at Day 6 of the nitrogen starvation. The separation occurred between LL (low-lipid: 86.1% at Outlet # 1) and LC (88.8% at Outlet # 2) at Day 9 of the nitrogen starvation. This device can be used for onsite monitoring; therefore, it has the potential to reduce biofuel production costs.

Keywords: cell sorting; dielectrophoresis; biofuel; microalgae; flow cytometry

1. Introduction

Microalgae technology continues to show promise for becoming a major source of renewable liquid transportation fuel in the coming decades [1–4]. Since biodiesel can be produced from biological lipids, the ability to grow algae reliably with high lipid content can possibly reduce the ultimate cost of the biodiesel produced [5,6]. There is a demand for a high throughput, label-free method for sorting cells based on lipid content [7]. The cytoplasmic conductivity of microalgae can be varied in a repeatable fashion by inducing lipid accumulation [8,9,10]. Consequently, microalgae are an ideal target for a continuous-flow screening device that utilizes dielectrophoresis for separation.

Dielectrophoresis refers to the motion of polarizable particles in a non-uniform electric field [11]. Conceptually, one can imagine the formation of a dipole within a neutral particle placed in an electric field. If the strength of the field is not spatially uniform, the dipole can be unbalanced leading to a net force developing on the particle [12]. If the particle is more polarizable than the medium, it will undergo positive DEP (pDEP) and tend toward regions with higher electric fields. Conversely, if the particle is less polarizable than the medium, it will undergo negative DEP (nDEP) and tend away from regions with higher electric fields [13,14].

DEP force, which is a function of intrinsic (size, shape, conductivity, and permittivity of the shell and cytoplasm) and extrinsic (frequency, magnitude, and phase) characteristics of the cells, can be used to separate cells [11]. To achieve separation, two conditions must exist: (1) a difference in the intrinsic dielectric properties of the populations to be sorted and (2) a set of extrinsic parameters that exploits that difference. Separations can be based on differences in the magnitude or the direction of the DEP force.

Direction of the DEP force depends on the frequency of the external AC electric field. Frequencies with no DEP response are called crossover frequencies where DEP force changes direction. At lower frequencies crossover depends primarily upon properties of the membrane, while at the higher frequencies it depends primarily upon properties of the interior of cell [8,9,14]. This has formed the basis for several devices that are capable of label-free sorting of cells [7,14–21]. The most common approach utilized to sort cells via DEP is to use the DEP force to move the cells laterally within a microchannel where the target cells are either pushed (nDEP) or pulled (pDEP) away from the rest of the population. The amount of separation achieved depends on the shape of the electric field gradient [21], separation length [22], and flow characteristics [23]. For an efficient binary separation, there should be a significant difference between frequencies where the DEP force exerted on the cells changes from negative to positive [21,24,25]. For example Yang et al, [24] used nDEP force to push the cells away to different levitation heights of the channel while pDEP forces trap them at the electrode edges. This phenomenon can be used as a basis for cell differentiation where the cells exit the channel at different timeframes [21,24]. However, trapping can affect separation throughput due to the unwanted binding of the cells to the electrode edges. In the literature, numerous strategies have been developed to generate that nonuniform electric field that is required to produce DEP force, such as (1) the use of planar electrodes [15,23,26], (2) the use of three-dimensional and sidewall electrodes [27,28], and (3) the use of insulating structures [29]. To the best of author's knowledge, there are few reports that explicitly examine and quantify higher frequency DEP separation of microalgae based on lipid content in a continuous-flow device. This is

most likely due to the fact that standard benchtop function generators are typically limited to a maximum frequency of 20 MHz [14,27,30,31,32].

In this paper, a DEP separation method using planar electrodes is developed. The basis for this design is that pDEP is typically stronger than nDEP due to the shape of the electric field gradients for the microalgae used in this study [10,11]. Therefore, nDEP is only used initially to push the high-lipid cells laterally away from the remaining cells. Once they are pushed far enough, they enter a region where the electric field gradient is not strong enough to move the cells and the hydrodynamic forces transfer them whereas the low-lipid cells are pulled along the electrode edges via the balance between pDEP relative to the hydrodynamic forces. To quantify the relative separation efficiency, sorted samples were labeled with BODIPY fluorescence dye and examined by flow cytometry.

2. Principles and Design

DEP motions can be theoretically described by the DEP force for homogenous spherical cells [11] (Equation 1):

$$F_{DEP} = 2\boldsymbol{\pi}\varepsilon_m R^3 Re\,(F_{CM})\,\boldsymbol{\nabla}E_{RMS}^2 \tag{1}$$

where $\mathbf{R}$ is radius of the particle and $\mathbf{E_{RMS}}$ is root mean squared of the electric field.

The frequency dependence of the DEP force is captured by the Clausius-Mossotti factor, $\mathbf{F_{CM}}$, which compares the frequency dependent complex permittivity (i.e., dielectric properties) of the particle to the medium (Equations 2 and 3). The actual form of $\mathbf{F_{CM}}$ also depends on the shape and complexity of the particle:

$$F_{CM} = \frac{(\varepsilon^*_p - \varepsilon^*_m)}{(\varepsilon^*_p + 2\varepsilon^*_m)} \tag{2}$$

$$\varepsilon^*_i = \varepsilon_i - \frac{j\sigma_i}{\omega} \tag{3}$$

where $\boldsymbol{\varepsilon_m}$ is medium permittivity and $\boldsymbol{\varepsilon_p^*}$ is complex permittivity of the particle.

The real part of Clausius-Mossotti factor, which takes on values from −0.5 to 1, determines the sign of the DEP force. The most commonly used model for the living cells is the single-shell model that considers a homogeneous cytoplasm surrounded by a thin membrane of low conductivity. Additional shells can be added to this model to include features such as the highly conductive nucleus or the presence of a cell wall [11,14,33]. Each layer represents an effective permittivity calculated with Equation 4:

$$\varepsilon^*_{peff} = \varepsilon^*_s \frac{(\frac{R+\delta}{R})^3 + 2\frac{(\varepsilon^*_c - \varepsilon^*_s)}{(\varepsilon^*_c + 2\varepsilon^*_s)}}{(\frac{R+\delta}{R})^3 - \frac{(\varepsilon^*_c - \varepsilon^*_s)}{(\varepsilon^*_c + 2\varepsilon^*_s)}} \tag{4}$$

where $\boldsymbol{\delta}$ is shell thickness, $\boldsymbol{\varepsilon_c^*}$ is complex permittivity of the cytoplasm, and $\boldsymbol{\varepsilon_s^*}$ is complex permittivity of the shell. To achieve clear separation, the operating regime should be identified. For single-shell particles, such as microalgae, electric fields with higher frequencies penetrate into the shield of the membrane; thus, dielectric properties of the cytoplasm determine the upper crossover frequency range [9,14]. It has been previously demonstrated that lipid content decreases conductivity

of the cytoplasm and shifts the upper crossover frequency to lower values [8,9,10]. Therefore, the shift in the upper crossover frequency of the high-lipid cells creates an operating regime where low-lipid cells have a pDEP response while high-lipid cells have an nDEP or noDEP response. Thus, microalgae cells can be continuously separated based on the effective conductivity of the cytoplasm, as dictated by lipid content in this operating regime. The DEP spectrum of the target cells has been explored with several time-course experiments and the results have been published in our previous work [9]. It was found that the optimal frequency generating a significant difference in $\boldsymbol{Re}\ (\boldsymbol{F_{CM}})$ of the high- and low-lipid *C. reinhardtii* cells is between 40-50 MHz. However, clear continuous-flow sorting requires a detailed analysis of the electric and hydrodynamic forces within the microfluidic channel.

From a throughput perspective, the channel needs to be as large as possible to maximize the flow rate within the channel and to increase the number of processed cells. On the other hand, a larger channel will require higher voltages to establish the necessary electric field gradients. As described by Song et al. [15], to improve sorting efficiency and throughput, an aligned planar, interdigitated electrode design has been used. The basis for this design is that pDEP is typically stronger than nDEP due to the value of the Clausius-Mossotti factor and the shape of the electric field gradients. The pDEP effect is used to attract low-lipid cells to the electrode edges. However, this can lead to cell trapping and can result in low separation throughput. To eliminate this problem, amplitude modulation mode was used to generate a pulsed AC electric field with a high frequency and V_{pp} signal. Low-lipid cells moved in a zigzag trajectory resulting from the balance between hydrodynamic (forward fluid drag) relative to the pDEP (along the electrode) forces [15,34,35]. The trajectories of the cells were confirmed by numerical simulation performed with COMSOL 5.1 Multiphysics, particle trajectories module (Figure. 1A). This simulation confirms that low-lipid cells are transferring in a zigzag trajectory to the outlet while high-lipid cells experience nDEP or noDEP and continue to flow near the wall of the channel. Gradient of the $\left|\boldsymbol{E^2}\right|$ values increases at the tip of the electrode. As a result, the cells with pDEP response are transported to the channel wall. Although numerical simulation had been carried out in 2D, the operating regime is more restricted in 2D since high-lipid cells must have noDEP (at the upper crossover frequency) response. Whereas, in the real 3D case high-lipid cells are repelled laterally from the planar electrodes due to the nDEP response and moved out of the effective DEP force gradient. Hence, either nDEP or noDEP cases transfer high-lipid cells to the same outlet and broaden the operating regime in this design.

The image of the fabricated device used in this study is given in Figure. 1B. The width and the length of the microfluidic channel were 1 mm and 7.5 mm respectively, and the channel depth was 20 μm. The width of the sample inlet and sheath flow were 330 μm and 850 μm respectively. The interdigitated electrode array contained 40 electrodes with 50 μm in width and a gap of 50 μm. Every set of 10 electrode arrays was placed with an 80 μm gap to reduce cells adherence to the edges.

3. Materials and Methods

3.1. Sample preparation

The cell wall-less *dw15-1* (referred to as parental strain) and *pgd1* mutant strain of *C. reinhardtii* (Michigan State University) were cultured from slant using TAP growth medium [36,37].

Separately, a nitrogen-free medium was prepared from the same recipe by omitting the ammonium chloride. The cells were grown at 27 °C with an 18/6 hr light/dark cycle and continuous air bubbling. After the cells had grown to a dense culture, both cultures were centrifuged, decanted, and rinsed with the N-free medium three times and then re-suspended in the N-free medium. The absence of nitrogen stresses the cells, retards cell growth, and promotes the accumulation of lipids within the cell [36,38]. Since the *pgd1* mutant accumulates half the lipids as the *dw15-1* [37], microalgae cells with different lipid content were prepared. After sufficient lipids had been accumulated in the cells, as determined by fluorescence microscopy, a portion of each culture was separately centrifuged, decanted, and rinsed with DEP medium three times. The DEP medium consisted of deionized water adjusted to 106 ± 1 μS/cm conductivity with potassium chloride as measured with an Extech Exstik II conductivity meter (Nashua, NH). The optimum DEP medium conductivity was selected according to the largest shift in the upper crossover frequency of the microalgae cells due to the lipid accumulation over the experiment period [39]. Glucose was then added (85 g/L) to raise the osmotic pressure of DEP medium without affecting its conductivity [4,40]. To avoid cell binding to the surface of the channel, 0.1% bovine serum albumin (Sigma-Aldrich, USA) was added to the DEP medium. Both samples were stained by adding 2.5 μl of BODIPY 505/515 (Invitrogen, Grand Island, NY) stock solution (5 mg/mL in dimethyl sulfoxide, stored frozen) to 1 mL of the cell suspension [41]. The lipid bodies inside high-lipid cells were labeled with BODIPY fluorescence by a diffusion-trap mechanism [41,42].

3.2. Device fabrication

The continuous-flow DEP screening device consists of two primary construction components: (1) patterned Cr/Au layer (thickness: 250A Cr/1000A Au), and (2) polydimethylsiloxane (PDMS, Dow Corning SYLGARD 184) channel. Interdigitated gold electrodes were patterned by standard photolithography of AZ 1518 (AZ Electronic Materials, USA) and wet etching procedures [43,44]. Dry film photoresist (DuPont Riston Special FX920) with 20 μm thickness was laminated on a smooth polished copper substrate (Sigma Aldrich, USA), exposed to UV light with the design mask, and patterned to create a mold for the microchannel. The liquid-phase PDMS, made in 10:1 weight ratio of polymer and curing agent, was poured on the mold and cured for 1 hr at 100 °C. The cured PDMS channel was then peeled off, trimmed, and the inlet and outlet holes were punched into the channel with a core sample punch (TED PELLA, Inc., Redding, CA). Both channel and electrodes were treated by atmospheric plasma (PVA Tepla America, Inc., Corona, CA), manually aligned under the microscope, and placed on a 100 °C hot plate for 1 hr to complete the bonding. The experiments were conducted immediately after the bonding since treating by atmospheric plasma activates the siloxane bonds on the glass and increases the hydrophilicity of the channel [45,46]. To avoid cell adhesion, the channel surface was coated for 1 hour with 0.3% bovine serum albumin (Sigma-Aldrich, USA).

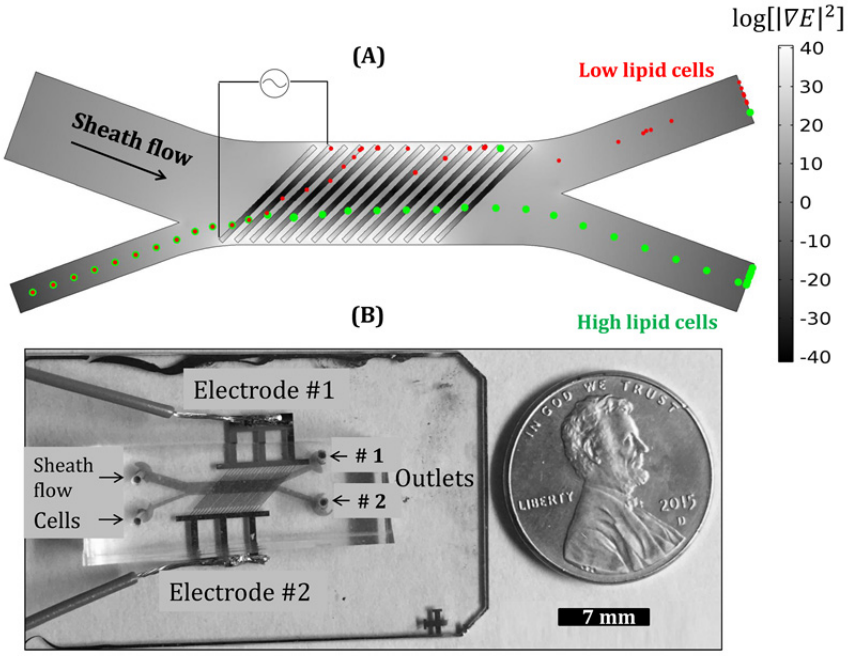

Figure 1. (A) Numerical simulation of cell trajectories in the DEP force field (parameters for the numerical simulation provided in S3 Table) (B) Micrograph of the fabricated continuous-flow DEP micro-separator.

3.3. Experimental set-up

The electronic set-up was connected to the DEP micro-separator by soldering wires to the electrode pads. A single syringe pump (KD Scientific, Inc., Holliston, MA) with two gas-tight glass syringes (1725 and 1750 Hamilton, USA) for main and sheath flow, respectively, was used to provide controlled main and sheath flows of the microalgae and DEP medium (Figure 2A) and minimized the variation in flow velocities. The syringes were connected to the inlet with 0.5 mm ID Tygon tubing (Cole-Parmer, Vernon Hills, IL).

Sine waves were generated with a Rigol D64162 signal generator (Oakwood Village, OH) capable of generating sine waves with frequencies up to 160 MHz and then amplified with an Ophir 5322 Rev.x1 RF (Los Angeles, CA) amplifier. A Fairview Microwave -3 dBm attenuator (Model SA3N511-03, Allen, TX) was placed between the amplifier and the electrodes to help match the load to the amplifier and reduce the amount of reflected power returning to the amplifier output [47]. This set-up was capable of generating electric fields with 30 V_{pp} amplitudes in the given frequency range as monitored by an oscilloscope (Model 1202 CA, Rigol Technologies) probing the electrodes. To generate on/off periods of high-frequency sine waves (20–80 MHz), the amplitude modulation mode on the function generator was used to modulate high-frequency sine wave as a 7 Hz square wave (Figure 2B).

Cells with different lipid contents were injected into the device at 3 µl/min and 6 µl/min of the main and sheath flow rate, respectively. A 50 MHz sine wave of 30 V_{pp} modulated on a 7 Hz, 50% duty cycle for on/off square wave, was used to create the DEP force acting on microalgae cells. Sorting was monitored by a color camera (Nikon DS-Fi1) and a UV-2A filter (Nikon; Excitation:

330–380, dichromatic mirror: 400, Emission: 420 nm cut-on) on an inverted epiflourescent microscope (Nikon TE-2000U). Since low- and high-lipid cells labeled with BODIPY 505/515 fluorescence dye are red and green, respectively, with the UV filter, the red channel was chosen to visualize bright, low-lipid cells in motion [48]. High-quality videos were analysed with the NIS-Element BR software. The experiments were conducted over 30 min periods and samples were collected for further analyses.

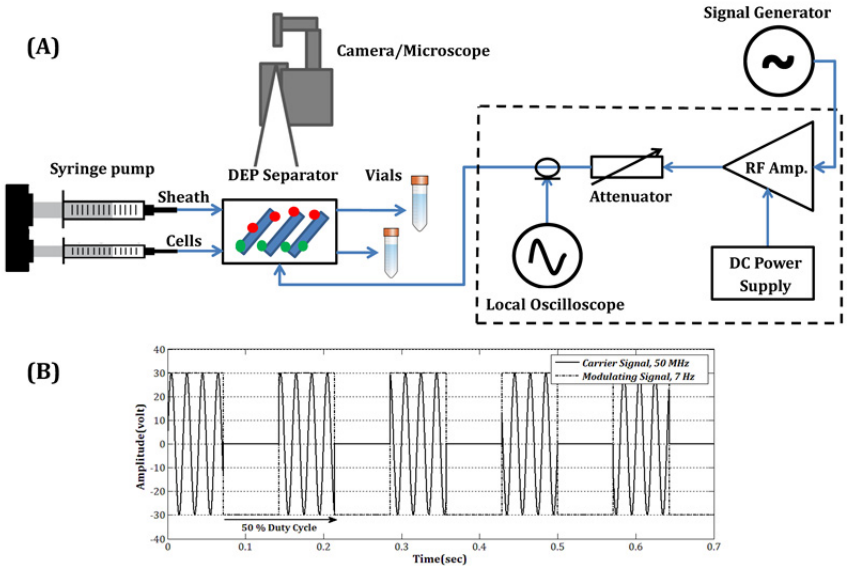

Figure 2. (A) Schematic of the experimental set-up (B) Amplitude modulation signal (frequency of the carrier signal is not to scale).

3.4. Verifying DEP separation with flow cytometry

C. reinhardtii dw15-1 (PS) and *pgd1* mutant (MU) cells were labeled with BODIPY 505/515 (4,4-Difluoro-1,3,5,7-Tetramethyl- 4-Bora-3a,4a-Diaza-s-Indacene, Life Technologies, Grand Island, NY, USA) and their fluorescence measured by flow cytometry. Samples were prepared by removing approximately 2 mL from the experimental culture and concentrating by the factor of 4. This ensured that enough cells were collected to be examined or high throughput achieved.

Collected, sorted samples from each outlet were labeled and then analysed with respect to the starting sample. To measure throughput, initial concentration of the PS and MU mixture was first measured by calculating the absolute count of the cells in the starting sample that was fed into the inlet. Using the absolute count of the staring sample and the flow rate of the main and sheath flow, the throughput of the continuous-flow screening device was measured. Flow cytometry samples were prepared by combining 1mL cell culture, 2.5 µL BODIPY 505/515 stock solution (5 mg/mL in dimethyl sulfoxide), and 50 µL BD Trucount absolute counting bead solution (BD Biosciences, San Jose, CA, USA); the BODIPY stock solution and counting bead solution were added in darkness to minimize photobleaching. Cellular fluorescence and scatter were measured using an LSR II flow cytometer (BD Biosciences, San Jose, CA, USA) equipped with 405-nm, 488-nm, 561-nm and

640-nm lasers. For each flow cytometry event, fluorescence through the following fluorescence filters was measured: FITC (530 ± 15 nm excited at 488 nm), APC (670 nm excited at 640 nm), and Pacific Blue (450 ± 25nm excited at 405 nm).

Cell events were gated according to their chlorophyll autofluorescence and the same gate was used for all starting and sorted samples. The fluorescence of the high-lipid cells labeled with BODIPY 505/515 was measured using the FITC filter. Approximately 10,000–50,000 total events were measured for each flow cytometry sample.

4. Results and Discussion

4.1. Particle separation experiments

To monitor the separation of the microalgae with different lipid content passing through an interdigitated electrode array, a screening device consisting of planar electrodes placed at 45º was used. The 20 μm height of the microchannel limits the DEP levitation height of the microalgae, thereby increasing the lateral pDEP force to facilitate lateral movement of the low-lipid cells [34]. DEP spectra of microalgae with different lipid content was analysed in the previous works for stationary DEP separation, and an optimum frequency of 42 MHz was obtained [9]. Thus, several frequency sweep experiments were carried out ranging from 40 MHz to 60MHz to characterize DEP spectra under continuous-flow separation conditions and an optimum frequency of 50 MHz was found to sort microalgae cells with different lipid content. Below 50 MHz, pDEP forces intend to trap low-lipid cells and above 50 MHz, these forces do not seem to be strong enough to create zigzag pattern.

Sorting experiments were conducted at a total flow rate of 9 μL/min (3 μL/min and 6 μL/min for the main and sheath flow inlets, respectively), along with an AC field of 30 Vpp at 50 MHz. A mixture of PS and MU cells were processed to demonstrate the separation of two distinctly different lipid contents via high frequency DEP, as MU accumulates half the lipid as PS [37]. Visual inspection confirmed that the microalgae cells with different lipid content were separated at the end of the channel and flowed out the different outlets (see video S1 in the supporting information). In the absence of electric field, both PS and MU flowed through the channel with no DEP deflection and exited via Outlet # 2 due to the laminar hydrodynamic focusing of the sheath flow (Figure 3A). The optimum frequency of 50 MHz is most suitable to separate PS from MU under these conditions because it results in strong pDEP for the low-lipid MU cells and nDEP or noDEP for the high-lipid PS cells. At this frequency, the pulsed AC electric field transferred the MU cells in zigzag trajectories to Outlet #1 (Figure 4), while the PS cells experiencing nDEP or noDEP continued down the channel and exited Outlet #2 (Figure 3B and C). Amplitude modulation mode generated an on/off pulsed wave to avoid cell trapping at the electrode edges while the cells were deflected laterally along the channel [15,34,49]. Cell trapping was minimized at 7 Hz frequency of the pulsed electric field during frequency sweep of the modulating signal. Clear separation was obtained with a throughput of 1000 cell/s after about 30 s. In this start-up lag, cell trajectories were stabilized avoiding output contamination in each outlet, which may have compromised separation efficiency. To achieve higher throughput, at least three factors must be satisfied: (1) significant difference in Re (F_{CM}) of microalgae cells with different lipid content at the optimum frequency [50], (2) the necessary electric gradient at the high frequency range, and (3) larger channel or higher flow rate.

Due to the relatively large size of the microalgae used in this study (10–15 μm), hydrodynamic forces must be maximized to avoid cell trapping, however the balance between DEP forces relative to the hydrodynamic forces determines the cell trajectories. Factors (2) and (3) are related; hence, larger channels are preferred as long as sufficient voltage can be provided. In this work, the channel dimension was chosen to be the smallest to ensure sufficient voltage can be provided. However a small channel will process few cells, in the experiments timeframe, resulting in a low throughput. Therefore flow rate was maximized to increase the number of the cells that can be processed [20].

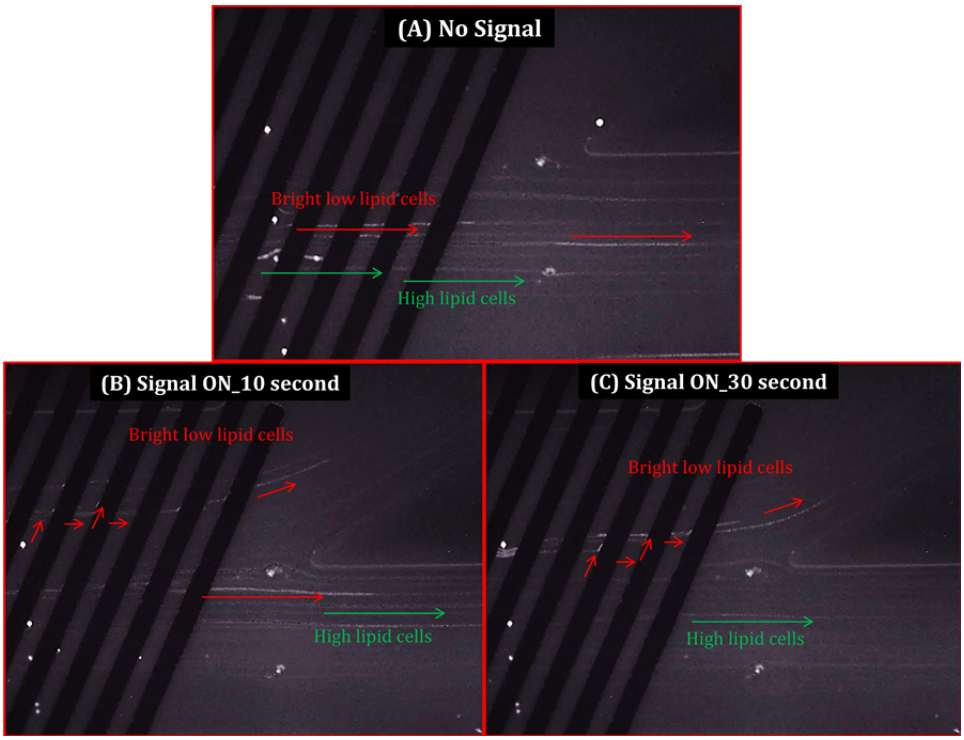

Figure 3. Micrograph of MU (Bright low-lipid cells) and PS (High-lipid cells) under a flow rate of 9 μl/min (A) No electric field (B) Field ON (AC field 50 MHz, 30 Vpp modulated on 7 Hz square wave) after 10 seconds (B) Field ON (AC field 50 MHz, 30 Vpp modulated on 7 Hz square wave) after 30 seconds.

4.2. Separation quantification

Collected samples were analysed by flow cytometer to evaluate the relative separation efficiency. Flow cytometry experiments confirmed that cells with higher lipid amounts exhibit greater BODIPY fluorescence per cells [51]. The cytogram of side scatter vs. FITC reveal that the population with greater FITC signal (intensity of the BODIPY staining that represents lipid amount) had greater side scatter (Figure 5A). The higher level of side scatter could be associated with cells with a higher level of cytoplasmic granularity [26,52]. Higher forward scatter also suggests that larger cells accumulate higher lipid content per cell, which is consistent with lipid accumulation increasing cell size [51,53,54]. However, the cytogram of forward scatter vs. BODIPY fluorescence demonstrated approximately the same range of cell size in cells with different lipid content (Figure 5B).

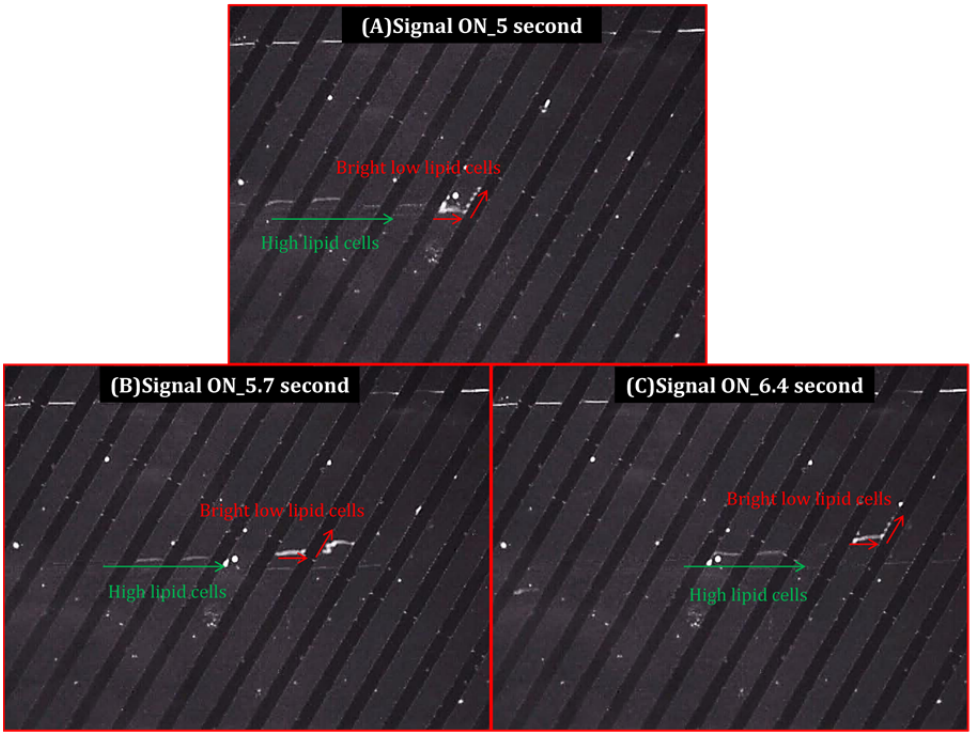

Figure 4. Micrograph of the zigzag cell trajectory of the low-lipid cells at different time-lapses in the 1 mm wide channel.

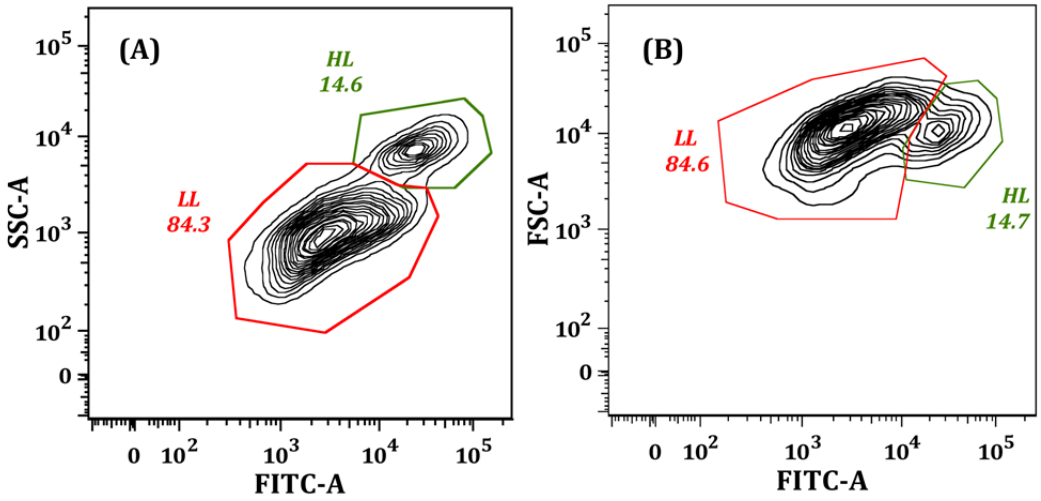

Figure 5. Flow cytometry measurements for high-lipid (HL) and low-lipid (LL) *C. reinhardtii* cells labeled with BODIPY at Day 6 of nitrogen starvation (A) Flow cytogram of side scatter vs. green fluorescence intensity (B) Flow cytogram of forward scatter vs. green fluorescence intensity.

Sensitivity of the separation performance was investigated with the time course series of experiments, as the lipid gradually accumulated over time. Both PS and MU cells have a similar growth pattern in that they reach the stationary phase by 3 days growth [54]. However, the duration of the stationary phase is different between strains. Thus, sorting was performed on Days 3, 6, and 9

of the nitrogen starvation, and collected samples were examined by flow cytometry (FCM). Chlorophyll auto-fluorescence is a biomarker for photosynthetic cells and enables an FCM gate for the separation analysis of the microalgae [52]. As a result, enrichment of the target cell population was measured by analysing the cytograms of APC-A (chlorophyll characteristic) vs. FITC (BODIPY fluorescence) and it was found that separation had not occurred at Day 3 (Figure 6). This may be due to the limited lipid bodies inside the cells. Therefore, there was not enough significant difference between Re (F_{CM}) of the PS and MU at the stationary phase (3d) to cause clear separation. At Day 6 (Figure7), two distinct populations of low- and high-lipid cells were transferred to Outlet#1 and Outlet #2 respectively. Starting from the late stationary phase, a low-chlorophyll population (LC) was observed in the nitrogen starved samples. A similar phenomenon possibly occurred with the work of Wang et al. [55], where the plasma membrane of the wall-less PS and MU had lysed but the lipid bodies maintained their spherical shape [55]. Thus, cells that lysed may lose their chlorophyll while lipid bodies remain whole (supporting information Figure S2). Despite the LC population, 74% enrichment was reached for the HL population at Outlet #2 (Figure 8A). The relatively low efficiency achieved on Day 6 may be due to the third LC population inside the original sample. At Day 9, the LC population accounted for 66.7% of the starting population (Figure 9A); hence, separation occurred between the LL and LC populations with a relative efficiency of 86.1% and 88.8% at Outlet#1 and Outlet#2 respectively (Figure 8B). Although the starting sample contained only 2.27% HL population at Day 9, the entire population had been sorted to Outlet#2 (Figure 9C), but the LC population had been enriched in the same outlet as the HL population (Figure 9C). Even though there is a significant difference between cytoplasmic properties of the LC and HL cells, both have nDEP or noDEP response in the high frequency electric field gradient of this design. In other words, LC cell cytoplasm has lower conductivity than the medium in 50 MHz frequency with the applied AC electric field. This confirms that LC cells are in fact HL cells, which have lost their

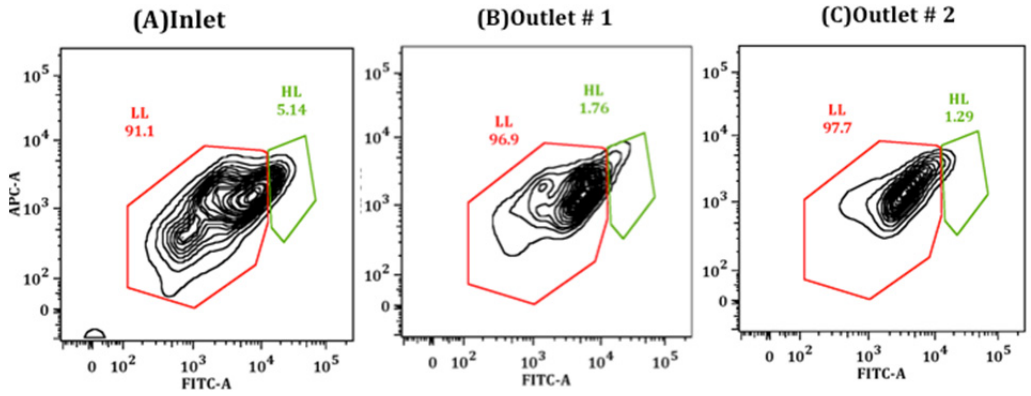

Figure 6. Separation did not occur at Day 3. Flow cytometry measurements of the PS and MU mixture strains before and after sorting at Day 3 of the nitrogen starvation (A) Flow cytogram of the chlorophyll characteristic (APC-A) vs. green fluorescence intensity (FITC-A) for the starting PS and MU mixture at the inlet (B) Flow cytogram of the chlorophyll characteristic (APC-A) vs. green fluorescence intensity (FITC-A) for collected sample at Outlet # 1 (C) Flow cytogram of the chlorophyll characteristic (APC-A) vs. green fluorescence intensity (FITC-A) for collected sample at Outlet # 2.

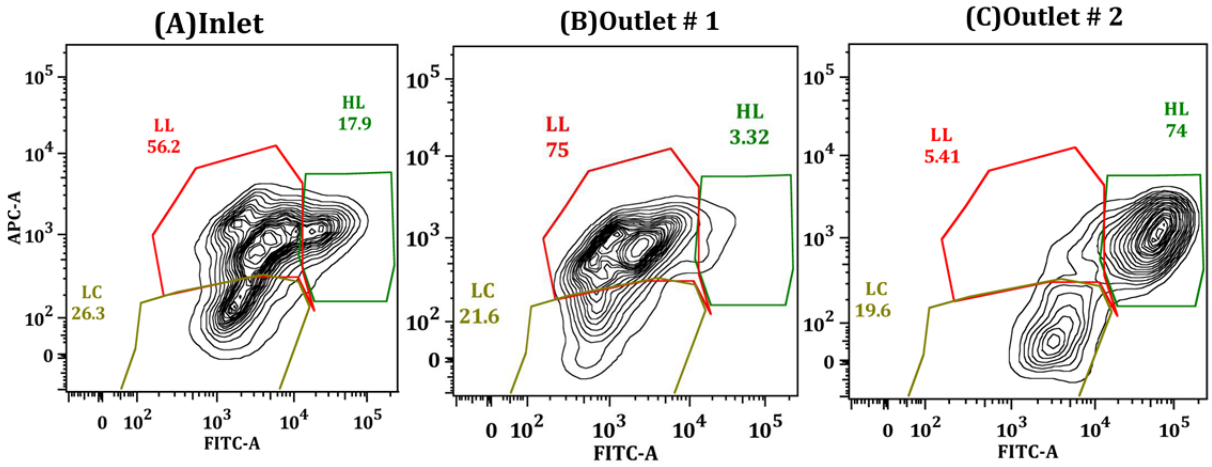

Figure 7. Separation occurred at Day 6 with 74% enrichment of the HL population. Flow cytometry measurements of the PS and MU mixture strains before and after sorting at Day 6 of the nitrogen starvation (A) Flow cytogram of the chlorophyll characteristic (APC-A) vs. green fluorescence intensity (FITC-A) for the starting PS and MU mixture at the inlet (B) Flow cytogram of the chlorophyll characteristic (APC-A) vs. green fluorescence intensity (FITC-A) for collected sample at Outlet # 1 (C) Flow cytogram of the chlorophyll characteristic (APC-A) vs. green fluorescence intensity (FITC-A) for collected sample at Outlet # 2.

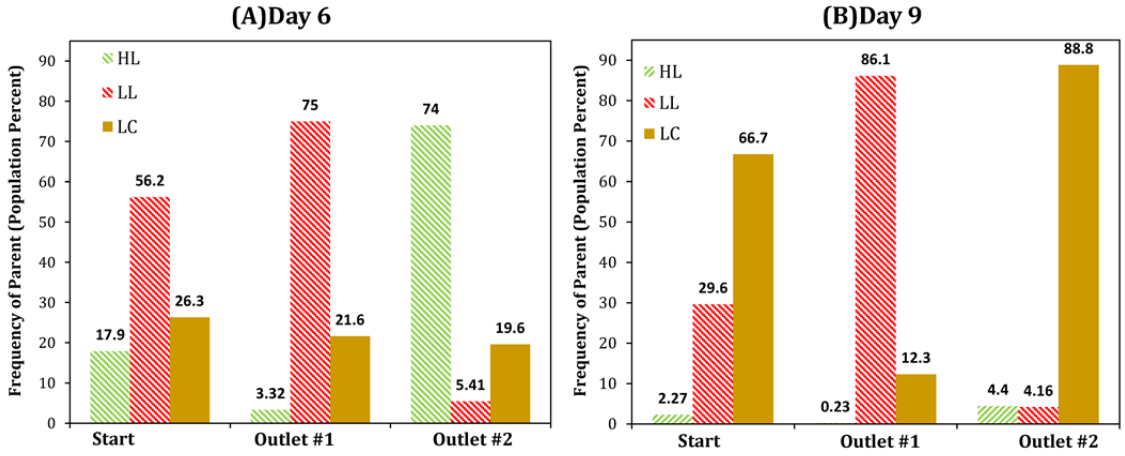

Figure 8. Relative separation efficiency of high-lipid (HL), low-lipid (LL) and low-chlorophyll (LC) cell populations at different outlets after sorting (A) At Day 6 of the nitrogen starvation (B) At Day 9 of the nitrogen starvation; The flow rate was 9 µl/min and the AC voltage was 30 Vpp at 50 MHz, modulated on square wave at 7 Hz.

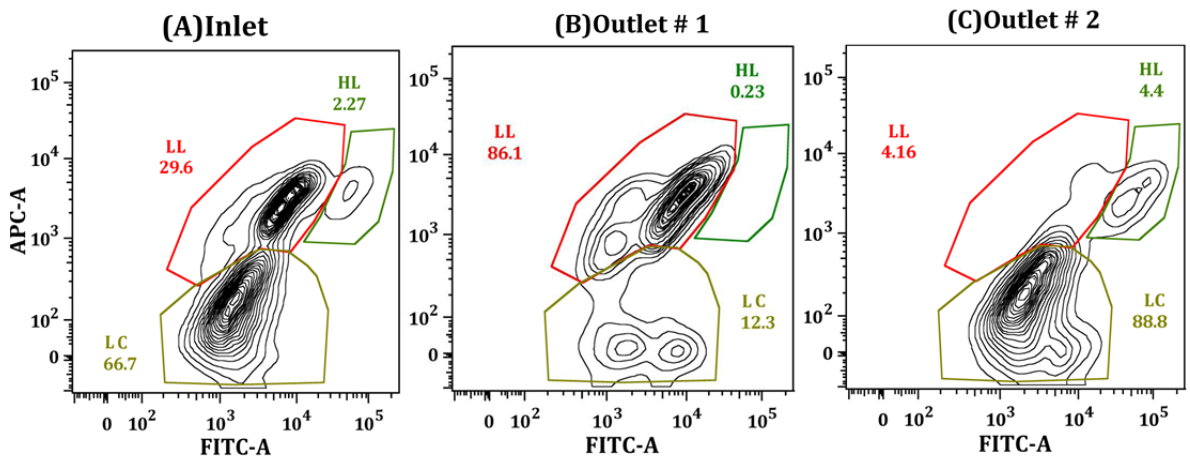

Figure 9. Flow cytometry measurements of the high-lipid (HL), low-lipid (LL) and low-chlorophyll (LC) cell populations before and after sorting at Day 9 of the nitrogen starvation (A) Flow cytogram of the chlorophyll characteristic (APC-A) vs. green fluorescence intensity (FITC-A) for the starting PS and MU mixture at the inlet (B) Flow cytogram of the chlorophyll characteristic (APC-A) vs. green fluorescence intensity (FITC-A) for collected sample at Outlet # 1 (C) Flow cytogram of the chlorophyll characteristic (APC-A) vs. green fluorescence intensity (FITC-A) for collected sample at Outlet # 2.

chlorophyll and a portion of lipid content. It is worth noting that lipid content was estimated by labeling with BODIPY fluorescence dye and intensity measurements [9]. Threshold was defined to distinguish high-lipid cells population based on the FITC signal from flow cytometer. According to the time-course experiments, it can be concluded that *C. reinhardtii* cells with different lipid content can be substantially separated at Day 6 with 74% relative efficiency via high frequency DEP. At this stage, the LC population had not been formed thoroughly; thus, binary separation can be attained.

5. Conclusions

In this study, a continuous-flow micro-separator device was fabricated and utilized for screening microalgae cells based on lipid content using interdigitated, planar electrode arrays. Higher frequency DEP response depends primarily on the dielectric properties of the cytoplasm; thus, it can be altered by lipid accumulation within the microalgae cells. Gradually accumulated lipid content at the early stationary phase (Day 6) provided a sufficient shift in DEP response of microalgae cells at higher frequencies to separate cells in the continuous-flow screening device. Optimum frequency (50 MHz) was found according to the largest throughput over the separation period. At the late stationary phase (Day 9) a low-chlorophyll population developed into the nitrogen-starved sample that compromised binary separation performance. At Day 3 of the nitrogen starvation, separation did not occur due to the insufficient lipid content resulting in a small difference between high frequency DEP responses of HL and LL populations. Therefore, DEP force was not strong enough relative to the hydrodynamic forces to differentiate and levitate cells based on their lipid content in continuous-flow sorting condition. Flow cytometry also verified the relative separation efficiency along with lipid accumulating inside the cells. The experimental results demonstrated that high frequency DEP,

as a non-invasive and label-free method, enabled the enrichment of the microalgae cells based on lipid content in the continuous-flow micro-separator device. This provides a lab tool for online culture monitoring that may facilitate biofuel production efforts.

Acknowledgements

This material is based upon work supported by the National Science Foundation (Grant No. 1265075). D. R. is partially supported by the Nevada INBRE (P20 GM103440) and the COBRE Phase III (P30GM110767).

Conflicts of Interest

All authors declare no conflicts of interest in this paper.

References

1. Hu Q, Sommerfeld M, Jarvis E, et al. (2008) Microalgal triacylglycerols as feedstocks for biofuel production: perspectives and advances. *Plant J* 54: 621–639.
2. Chisti Y (2008) Biodiesel from microalgae beats bioethanol. *Trends Biotechnol* 26: 126–131.
3. Dismukes GC, Carrieri D, Bennette N, et al. (2008) Aquatic phototrophs: efficient alternatives to land-based crops for biofuels. *Curr Opin Biotech* 19: 235–240.
4. Sharif H, Salleh A, Boyce AN, et al. Biodiesel Fuel Production from Algae as Renewable Energy. *Am J Bioch Biotechnol 2008* 4: 250–254.
5. Hannon M, Gimpel J, Tran M, et al. (2010) Biofuels from algae: challenges and potential. *Curr Opin Biotech* 21: 277–286.
6. Bono MS, Ahner BA, Kirby BJ (2013) Detection of algal lipid accumulation due to nitrogen limitation via dielectric spectroscopy of Chlamydomonas reinhardtii suspensions in a coaxial transmission line sample cell. *Bioresource Technol* 143: 623–631.
7. Deng YL, Kuo MY, Juang YJ (2014) Development of flow through dielectrophoresis microfluidic chips for biofuel production: Sorting and detection of microalgae with different lipid contents. *Biomicrofluidics* 8: 064120–064120.
8. Hadady H, Montiel C, Wetta D, et al. (2015) Liposomes as a model for the study of high frequency dielectrophoresis. *Electrophoresis* 36: 1423–1428.
9. Hadady H, Wong JJ, Hiibel SR, et al. (2014) High frequency dielectrophoretic response of microalgae over time. *Electrophoresis* 35: 3533–3540.
10. Michael KA, Hiibel SR, Geiger EJ (2014) Dependence of the dielectrophoretic upper crossover frequency on the lipid content of microalgal cells. *Algal Research* 6: 17–21.
11. Gagnon ZR (2011) Cellular dielectrophoresis: applications to the characterization, manipulation, separation and patterning of cells. *Electrophoresis* 32: 2466–2487.
12. Hoettges KF (2009) Dielectrophoresis as a Cell Characterisation Tool. *Microengineering in Biotechnology, Meth Mol Biol*. New York. NY: Humana Press, 183–198.
13. Hughes MP (2002) Strategies for dielectrophoretic separation in laboratory-on-a-chip systems. *Electrophoresis* 23: 2569–2582.

14. Gagnon Z, Gordon J, Sengupta S, et al. (2008) Bovine red blood cell starvation age discrimination through a glutaraldehyde-amplified dielectrophoretic approach with buffer selection and membrane cross-linking. *Electrophoresis* 29: 2272–2279.
15. Song H, Rosano JM, Wang Y, et al. (2015) Continuous-flow sorting of stem cells and differentiation products based on dielectrophoresis. *Lab Chip* 15: 1320–1328.
16. Valero A, Braschler T, Demierre N, et al. (2010) A miniaturized continuous dielectrophoretic cell sorter and its applications. *Biomicrofluidics* 4: 1–22.
17. Gossett DR, Weaver WM, Mach AJ, et al. (2010) Label-free cell separation and sorting in microfluidic systems. *Anal and Bioanal Chem* 397: 3249–3267.
18. Mernier G, Piacentini N, Braschler T, et al. (2010) Continuous-flow electrical lysis device with integrated control by dielectrophoretic cell sorting. *Lab Chip* 10: 2077–2082.
19. Vahey MD, Voldman J (2008) An Equilibrium Method for Continuous-Flow Cell Sorting Using Dielectrophoresis. *Anal Chem* 80: 3135–3143.
20. Hu X, Bessette PH, Qian J, et al. (2005) Marker-specific sorting of rare cells using dielectrophoresis. *Pnas* 102: 15757–15761.
21. Wang X-B, Yang J, Huang Y, et al. (2000) Cell Separation by Dielectrophoretic Field-flow-fractionation. *Anal Chem* 72: 832–839.
22. Moon HS, Kwon K, Kim SI, et al. (2011) Continuous separation of breast cancer cells from blood samples using multi-orifice flow fractionation (MOFF) and dielectrophoresis (DEP). *Lab Chip* 11: 1118–1125.
23. Doh I, Cho YH (2005) A continuous cell separation chip using hydrodynamic dielectrophoresis (DEP) process. *Sensor Actuat A-Phys* 121: 59–65.
24. Yang J, Huang Y, Wang XB, et al. (1999) Cell Separation on Microfabricated Electrodes Using Dielectrophoretic/Gravitational Field-Flow Fractionation. *J Am Chem Soc* 71: 911–918.
25. Lewpiriyawong N, Yang C (2013) Dielectrophoresis Field-Flow Fractionation for Continuous-Flow Separation of Particles and Cells in Microfluidic Devices. *Advances in Transport Phenomena 2011*. Switzerland: Springer International Publishing, 29–62.
26. Pommer MS, Zhang Y, Keerthi N, et al. (2008) Dielectrophoretic separation of platelets from diluted whole blood in microfluidic channels. *Electrophoresis* 29: 1213–1218.
27. Cheng IF, Chang HC, Hou D (2007) An integrated dielectrophoretic chip for continuous bioparticle filtering, focusing, sorting, trapping, and detecting. *Biomicrofluidics* 1: 21503–21515.
28. Piacentini N, Mernier G, Tornay R, et al. (2011) Separation of platelets from other blood cells in continuous-flow by dielectrophoresis field-flow-fractionation. *Biomicrofluidics* 5: 034122–034128.
29. Cima I, Yee CW, Iliescu FS, et al. (2013) Label-free isolation of circulating tumor cells in microfluidic devices: Current research and perspectives. *Biomicrofluidics* 7: 011810–011813.
30. Deng YL, Chang JS, Juang YJ (2013) Separation of microalgae with different lipid contents by dielectrophoresis. *Bioresource Technol* 135: 137–141.
31. Schor AR, Buie CR (2012) Non-Invasive Sorting of Lipid Producing Microalgae With Dielectrophoresis Using Microelectrodes. ASME 2012 International Mechanical Engineering Congress and Exposition. Houston, Texas: American Society of Mechanical Engineers, 701–707.
32. Schor AR, Buie CR (2015) Dielectrophoretic sorting of lipid-containing microorganisms using high frequency electric fields produced by conducting post arrays. Solid-State Sensors, Actuators

and Microsystems (TRANSDUCERS), 2015 Transducers - 2015 18th International Conference on. Anchorage, AK: IEEE, 1617–1620.
33. Broche LM, Labeed FH, Hughes MP (2005) Extraction of dielectric properties of multiple populations from dielectrophoretic collection spectrum data. *Phys Med Biol* 50: 2267–2274.
34. Han KH, Frazier AB (2008) Lateral-driven continuous dielectrophoretic microseparators for blood cells suspended in a highly conductive medium. *Lab Chip* 8: 1079–1086.
35. Shima HC, Kwaka YK, Hanb CS, et al. (2009) Effect of a square wave on an assembly of multi-walled carbon nanotubes using AC dielectrophoresis. *Physica E: Low-dimensional Systems and Nanostructures* 41: 1137–1142.
36. Rodolfi L, Chini Zittelli G, Padovani G, et al. (2014) Microalgae for oil: Strain selection, induction of lipid synthesis and outdoor mass cultivation in a low-cost photobioreactor. *Biotechnol Bioeng* 102: 100–112.
37. Li X, Moellering ER, Liu B, et al. (2012) A Galactoglycerolipid Lipase Is Required for Triacylglycerol Accumulation and Survival Following Nitrogen Deprivation in Chlamydomonas reinhardtii. *The Plant Cell* 24: 4670–4686.
38. Sheehan J, Dunahay T, Benemann J, et al. (1998) Look back at the U. S. Department of Energy's Aquatic Species Program: Biodiesel from Algae. U.S. Department of Energy's Office of Fuels Development.
39. Hadady H, Wong JJ, Hiibel SR, et al. (2014) Effect of Media Conductivity on High Frequency Dielectrophoretic Response. ASME 2014 International Mechanical Engineering Congress and Exposition. Montreal, Quebec, Canada: American Society of Mechanical Engineers. V010T013A006.
40. Hoettges KF, Hubner Y, Broche LM, et al. (2008) Dielectrophoresis-activated multiwell plate for label-free high-throughput drug assessment. *Anal Chem* 80: 2063–2068.
41. Cooper MS, Hardin WR, Petersen TW, et al. (2010) Visualizing "green oil" in live algal cells. *J Biosci Bioeng* 109: 198–201.
42. Akimoto S, Mimuro M (2007) Application of Time-Resolved Polarization Fluorescence Spectroscopy in the Femtosecond Range to Photosynthetic Systems. *J Photoch Photobio* 83: 163–170.
43. Xia Y, Whitesides GM (2003) SOFT LITHOGRAPHY. *Annu Rev Mater Sci* 28: 159–184.
44. Geiger EJ, Pisano AP, Svec F (2010) A Polymer-Based Microfluidic Platform Featuring On-Chip Actuated Hydrogel Valves for Disposable Applications. *J Microelectromech S* 19: 944–950.
45. Aran K, Sasso LA, Kamdar N, et al. (2010) Irreversible, direct bonding of nanoporous polymer membranes to PDMS or glass microdevices. *Lab Chip* 10: 548–552.
46. Gesche R, Kovacs R, Scherer J (2005) Mobile plasma activation of polymers using the plasma gun. *Surf Coat Tech* 200: 544–547.
47. Hadady H, Michael KA, Geiger EJ (2014) Impedance Effects During High–Frequency Dielectrophoresis. ASME 2014 International Mechanical Engineering Congress and Exposition. Montreal, Quebec, Canada: American Society of Mechanical Engineers, V010T013A046.
48. Mooij PR, Stouten GR, Tamis J, et al. (2013) Survival of the fattest. *Energ Environ Sci* 6: 3404–3406.
49. Ling SH, Lam YC, Chian KS (2012) Continuous Cell Separation Using Dielectrophoresis through Asymmetric and Periodic Microelectrode Array. *Anal Chem* 84: 6463–6470.

50. Hadady H, Hiibel SR, Redelman D, et al. (2015) Use of a Separability parameter for the Design of a High Frequency Dielectrophoresis Cell Sorter Device. InterPACK/ICNMM2015. California.
51. Bono MS, Garcia RD, Sri-Jayantha DV, et al. (2015) Measurement of Lipid Accumulation in Chlorella vulgaris via Flow Cytometry and Liquid-State Â¹H NMR Spectroscopy for Development of an NMR-Traceable Flow Cytometry Protocol. *Plos One* 10: 1–18.
52. Hyka P, Lickova S, Přibyl P, et al. (2013) Flow cytometry for the development of biotechnological processes with microalgae. *Biotechnol Adv* 31: 2–16.
53. Montero MF, Aristizábal M, Reina GG (2011) Isolation of high-lipid content strains of the marine microalga Tetras. *J Appl Phycol* 23: 1053–1057.
54. Velmurugan N, Sung M, Yim SS, et al. (2013) Evaluation of intracellular lipid bodies in Chlamydomonas reinhardtii strains by flow cytometry. *Bioresource Technol* 138: 30–37.
55. Wang ZT, Ullrich N, Joo S, et al. (2009) Algal Lipid Bodies: Stress Induction, Purification, and Biochemical Characterization in Wild-Type and Starchless Chlamydomonas reinhardtii. *Eukaryot Cell* 8: 1856–1868.

AIMS Press